SEPARATION CONTROL BY ACOUSTIC EXCITATION ON HIGHLY LOADED LOW PRESSURE TURBINE BLADES

C. Bernardini[†] *– S. I. Benton*[‡] *– J. P. Bons*[‡]

[†]Department of Energy Engineering, University of Florence, Florence, Italy
currently visiting at Department of Mechanical and Aerospace Engineering,
The Ohio State University, Columbus, Ohio, U.S.A.
bernardini.3@osu.edu

[‡] Department of Mechanical and Aerospace Engineering,
The Ohio State University, Columbus, Ohio, U.S.A.
benton.53@osu.edu – bons.2@osu.edu

ABSTRACT

Flow control is a valuable route to overcome laminar separation in highly loaded low-pressure turbine blades at low Reynolds number. The present work aims to explore the possibility of flow control by external acoustic excitation, which provides further insight into the mechanisms that can be exploited for control. Two blade profiles with aft- and front-loaded velocity distributions have been tested in a low-speed wind tunnel. A loudspeaker is mounted atop the tunnel, upstream of the inlet section. Wake loss surveys show that the most effective frequencies of the excitation are found to be in the range of the fundamental frequency of the separated shear layer. Particle image velocimetry data show that perturbations at this frequency enhance coherence of vortices shed from the separating shear layer, which increases momentum exchange thus favoring separation reduction. Although best effectiveness is accomplished with low turbulence level, sound control is still effective even with an engine representative level, particularly for the aft-loaded profile.

NOMENCLATURE

C_x	Axial chord
f	Frequency
k	Wavenumber
n	Time series counter
N	Total number of wavenumbers
$P_{T,in}$	Inlet total pressure
$P_{T,out}$	Exit total pressure
$P_{S,in}$	Inlet static pressure
Re	Reynolds number based on axial chord and outlet velocity
S	Pitch
Sw	Swirl strength parameter
s	Pitch direction
s_w	Wavelet scale
Tu	Turbulence intensity
u'	x-velocity fluctuations
$U_{x,in}$	Inlet axial velocity
$U_{x,out}$	Exit axial velocity
U_e	Nominal exit freestream velocity
$\hat{x}_k$	Fourier transform of data signal
Zw	Zweifel coefficient

α_{in}	Inlet metal angle
α_{out}	Exit metal angle
γ	Pitchwise integrated wake loss coefficient
δ_t	Time spacing between data points
Δu	Velocity fluctuations amplitude at excitation frequency
Ψ	Wavelet function
$\widehat{\Psi}^*$	Complex conjugate of wavelet function Fourier transform
ω_k	Wavelet frequency
ω_z	Spanwise vorticity

INTRODUCTION

Modern high by-pass ratio engines require high work output from the low-pressure turbine (LPT) which usually drives the fan. Recent trends of low blade count with high single blade loading provide the expected performance of LPT stages. However, this trend toward ever higher blade loading presents the downside of susceptibility to stall on the suction side when the Reynolds number falls to low values, as might occur in cruise conditions for aero-engines (Hodson and Howell, 2005). Moreover, efforts on improving the LPT stages performance have led research to address the effect of velocity distribution on the blade suction side. Studies by Howell et al. (2001) and Corriveau and Sjolander, (2004), have demonstrated that moving velocity peak further aft would increase the suction surface length over which the boundary layer remains laminar thus reducing profile losses. However highly aft-loaded profiles more easily undergo large open separation at low Reynolds number even under the effect of unsteady wakes (Bons et al, 2012). Flow control techniques are therefore considered a valuable route to overcome this issue. Many studies have been carried out employing different types of flow control, including passive trips, steady blowing, normal or angled vortex generator jets (VGJs) and synthetic jets. Bons et al. (2002) postulated that VGJ effectiveness relies on both generation of vortical structures able to carry high-momentum fluid towards the wall and excitation of the most unstable shear layer modes (Postl et al., 2011). The most unstable mode can be found analytically from the Rayleigh equation and represents the instability wave with highest amplification rate. (Michalke, 1965). The frequency that characterizes this mode is the most unstable frequency. The transition process leading to reattachment of a laminar separation bubble is initiated by growth of fluctuations at the most unstable mode in the separating shear layer. Watmuff (1999) showed that these inviscid Kelvin-Helmholtz (K-H) wave packets amplify and eventually roll up into vortices which later break down into turbulence in the reattaching portion of the bubble.

The present study aims to explore the ability of acoustic excitation to control separation by exploitation of shear layer instability. Recent studies have adopted actuators pulsating at the most unstable frequencies (Baumann et al., 2011) however using pure sound isolates the effect of excited instabilities from any massflow introduced into the boundary layer. Sound control has been adopted to control separation on airfoils, as shown by Zaman, (1992) and Greenblatt and Wygnanski, (2000). Yarusevich et al. (2007) explored the effect of frequency excitation on a stalled airfoil and observed that the transition process is accelerated by high-amplitude excitation at the instability frequency. However, there is a threshold amplitude at which a closed separation is recovered, beyond which no further improvement occurs. This work investigates the ability to control separation with excitation at frequencies in the range of the shear layer instability in a front and an aft highly loaded LPT profile at low Reynolds number. A low turbulence level is first adopted to allow the predominance of the excited frequency. A higher *Tu* level is considered as well to verify the validity of this approach in engine representative conditions.

EXPERIMENTAL SETUP

The facility used is a low-speed open-loop wind tunnel powered by a centrifugal blower. The freestream turbulence at the cascade inlet, after a series of flow conditioners, is 0.3% (low-*Tu*) and is increased to 3% (high-*Tu*) by means of a round bar turbulence grid placed 1.35 m upstream of the inlet. For the two blade profiles used, a three passage cascade is set up as depicted in Figure 1. Data are acquired over the center of the blade span, where the flow was shown to be approximately two-dimensional (Benton et al, 2013), at Reynolds number 30,000 based on the nominal (isentropic) exit velocity. The flow field is characterized by ambient temperature and pressure and an inlet velocity of about 2.2 m/s.

Two blade profiles have been investigated, the first one has a front-loaded velocity distribution (which will be called hereafter Blade-F) while the second one is aft-loaded (Blade-A). A sketch of the two profile shapes is shown in Figure 1-left (the profiles are slightly modified for confidentiality reasons). The Zweifel coefficient, which is defined as

$$Zw = 2\frac{S}{C_x}\cos^2\alpha_{out}\left(\tan\alpha_{out} + \frac{U_{x,in}}{U_{x,out}}\tan\alpha_{in}\right) \qquad [1]$$

is equal to 1.59 for Blade-F and 1.34 for Blade-A. The diffusion factor $[(U_{max}-U_e)/U_e]$ is about 57% for Blade-F and about 53% for Blade-A. Peak loading for Blade-F and Blade-A occur at 25% and 58% axial chord, respectively. The inlet and exit metal angles are respectively 35º and 60º for both profiles.

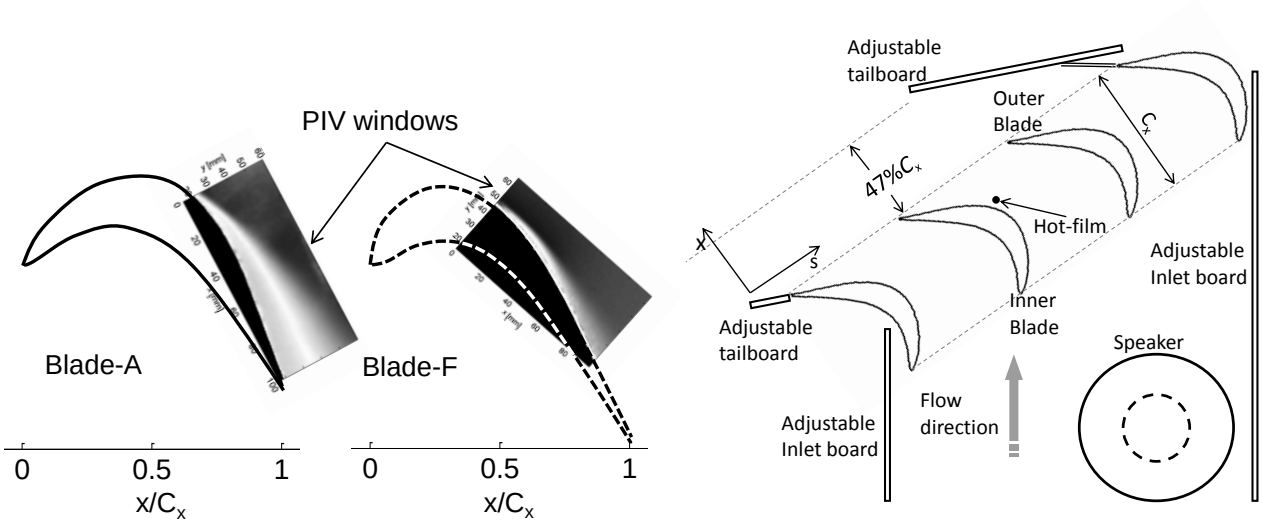

Figure 1. Sketch of blade profiles (left) with PIV window location; schematic of the wind tunnel (right)

Total pressure losses were collected in the pitchwise direction 47% C_x downstream of the exit section. A Kiel probe with a 3.2 mm sensing head is adopted referenced to an inlet pitot probe. The pitchwise integrated wake loss coefficient is defined in Eq. 2.

$$\gamma = \frac{1}{S}\int_{-S/2}^{S/2}\left(\frac{P_{T,in}-P_{T,out}}{P_{T,in}-P_{S,in}}\right)ds \qquad [2]$$

Uncertainty in the pressure measurement translates to an uncertainty of ±1.5% in the integrated wake loss coefficient γ and ±2.1% in the normalized value shown hereafter. Velocity signals have been acquired by means of a single element hot-film anemometer (TSI 1210-20) at 70% C_x at a distance from the wall corresponding to the negative peak skewness of the velocity signal. The hot-

film signal was sampled for 30 s at 20 kHz and filtered at 10 kHz for anti-aliasing. A single-camera LaVision particle image velocimetry (PIV) system was used to take two-dimensional velocity data at midspan plane. The CCD (charge-coupled device) camera has a resolution of 1376 by 1040 pixels and was mounted atop the test section. The camera window was set to capture the separated shear layer on the suction surface of the inner blade. The PIV window extends from about 48% C_x to 85% C_x, for Blade-F and from about 65% C_x to the trailing edge for Blade-A. These locations are represented in Figure 1-left relative to both blade profiles with sample PIV images. PIV data is presented in the camera coordinate system. A Nd:YAG laser was mounted to a three-axis traverse on one side of the test section and used to project two consecutive laser sheets in the x-y plane with 75 μs time separation for *Re* = 30,000. The PIV data was reduced to produce converged time-mean statistics over 1000 instantaneous images. The image acquisition was then phase-locked to the transistor-transistor logic (TTL) signal from the signal generator driving the speaker to acquire phase-locked data for five phases in an acoustic wave period. Ensemble-averaged statistics were produced from over 1000 instantaneous images.

Acoustic Characterization

A 6-1/2'' 2-way speaker with a frequency response from 65 Hz to 22,000 Hz was used to accomplish flow control by discrete acoustic tones. The speaker was flush-mounted in the top wall of the duct section, its center located at 0.18 m upstream of the inlet section between the outer and inner blade, as shown in Figure 1. The speaker was connected to an amplifier which was driven by a signal generator. The amplitude of the voltage delivered to the speaker can be adjusted by the amplifier and refined by the signal generator. The speaker excitation amplitude Δu_f corresponds to the amplitude of the Fourier transform (at the excited frequency) of the velocity measured by a hot-film in the passage freestream just downstream of the leading edge at the blade midspan. For a constant voltage applied to the speaker the amplitude of the velocity fluctuations is not constant and degrades with increasing frequency (an example is given in Figure 2-left). Therefore, in order to be able to independently tune amplitude and frequency, for each tested frequency and for both turbulence levels five velocity measurements have been recorded at increasing input voltage. Based on the spline interpolation, the voltage has then been adjusted in order to give the same velocity fluctuation for each frequency. The right plot of Figure 2 shows an example of this process for two frequencies in the high-*Tu* case. In the remainder, the acoustic excitation amplitude is normalized by the inlet velocity U_{in} and is referred to as $\Delta u_f/U_{in}$.

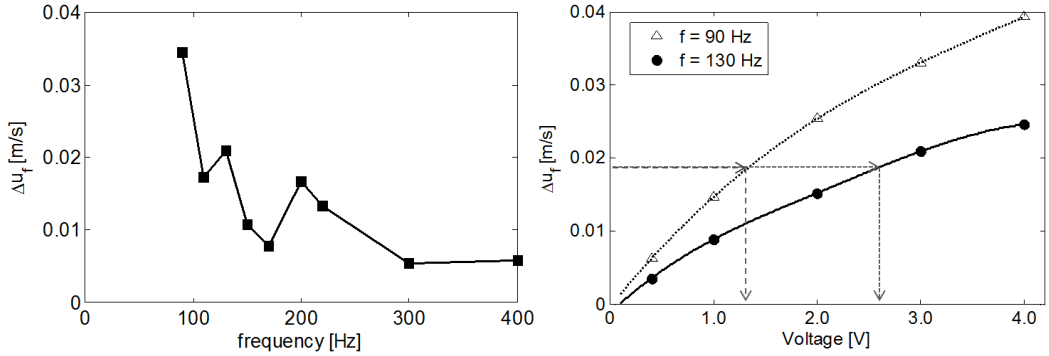

Figure 2. Amplitude of velocity fluctuation at excitation frequency at constant voltage (left) and at constant frequency (right).

Data analysis

Wavelet Analysis

Wavelet analysis is a technique first made popular in turbulence research by Farge (1992). The technique correlates a prescribed wavelet function Ψ with a given data signal to allow for

computation of the frequency spectra on a time accurate basis. The wavelet spectra are computed as shown in Eq. 3, where $\hat{x}_k$ is the Fourier transform of the data signal.

$$W_n(s_w) = \sum_{k=0}^{N-1} \hat{x}_k \hat{\psi}^*(s_w \omega_k) e^{i\omega_k n \delta t} \quad [3]$$

The method is formulated as described by Torrence and Compo (1998) and is implemented using portions of the code provided by the authors. In this study, the Morlet wavelet function was chosen for its increased accuracy in the frequency domain. Although this does increase uncertainty in the temporal resolution it was deemed important in this study to verify that the frequencies were in the range of excited frequencies.

Swirl Strength

In a complicated flow field, regions of considerable shear stress may conceal large-scale structures, thus making the identification of these structures difficult to determine. A useful way of unveiling these structures is the use of the swirl strength parameter from PIV data. The swirl strength is calculated from the eigen-analysis of the velocity gradient tensor, whereby the eigenvalues are the principle strain rates that determine the local flow topology (Adrian et al., 2000). For the data acquired, there are either two real eigenvalues or a complex conjugate pair. The sign of the real part determines whether the flow diverges or converges on a given point in the flow field. The magnitude of the imaginary part of the eigenvalue determines the swirl strength Sw. Zhou et al. (1999) offer a detailed explanation for this result. Regions of significant swirl strength tend then to appear in a distinct circular region of a vortex core.

RESULTS

Acoustic Control on Blade-F with Low-*Tu*

The Blade-F profile presents a large open separation at Re = 30,000 (Bernardini et al., 2012). The most amplified frequency in the shear layer is a band centered on f = 110 Hz from the power spectral density (PSD) of the uncontrolled case for both levels of turbulence intensity. Acoustic excitation at different frequencies and constant amplitude of $\Delta u_f/U_{in}$ = 0.5% is applied. Since the speaker performance decays slightly at higher frequencies, this amplitude is chosen to maintain a common value for all frequencies investigated. The effect of control is summarized in Figure 3-left, which shows the integrated wake loss coefficient normalized by the uncontrolled case. It is apparent that the most effective frequencies fall in the range of the most amplified frequencies in the shear layer (grey band) with a reduction of about 40% in the loss. In Figure 3-right the effect of control at f = 110 Hz at increasing excitation amplitude level is documented. Increasing the amplitude of fluctuations from low values brings positive effects on losses, thus progressively reducing separation size. However there is a threshold amplitude beyond which no further gain is achieved. This result was also observed by Yarusevich et al. (2007). These results suggest that a linear stability mechanism is exploited, that is the most unstable mode is fed until it is completely saturated.

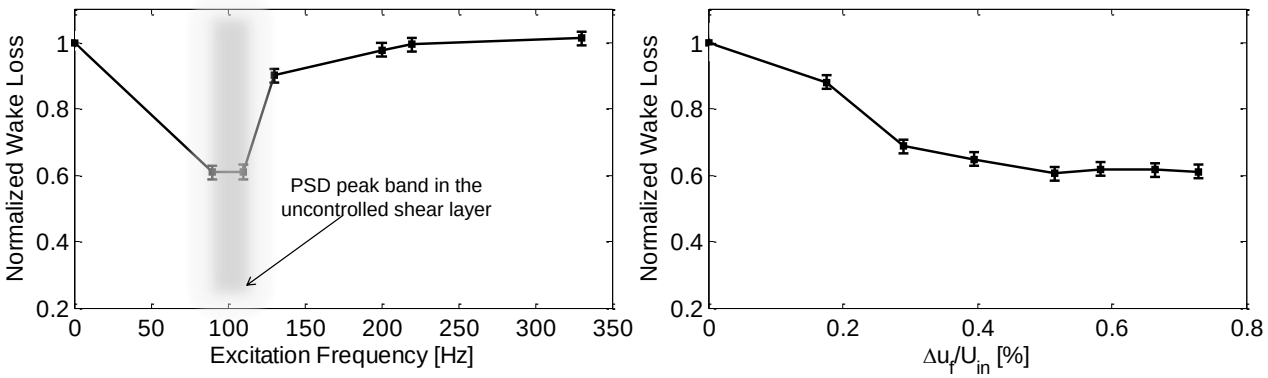

Figure 3. Integrated wake loss coefficient normalized by the uncontrolled case for Blade-F, Low-*Tu*. Left: excitation frequency effect. Right: amplitude effect, control at *f* = 110 Hz.

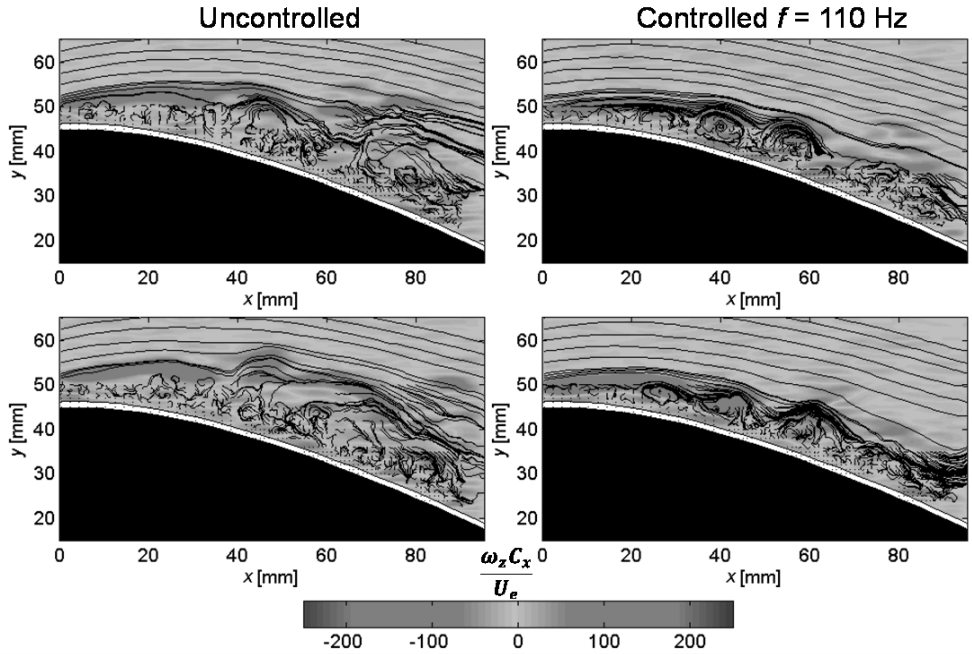

Figure 4. Instantaneous PIV images at two instants for Blade-F, Low-*Tu*: streamlines superposed on normalized spanwise vorticity contours ($\omega_z C_x/U_e$). Left column: uncontrolled; right column: control at *f* = 110 Hz.

The mechanism by which sound control is able to reduce separation is investigated through instantaneous PIV data. Figure 4 shows streamlines superposed to spanwise normalized vorticity magnitude at two randomly picked instants without control (left) and with control at f = 110 Hz (right). Although roll-up vortices shed from the upper edge of separation are still recognizable at some instants in the uncontrolled case, they are less organized and frequently break down into random turbulent fluctuations far from the wall, before they have time to grow and entrain high momentum fluid.

By contrast, in the controlled case at least two coherent structures are present at all times before they breakdown to turbulence. Coherence of vortex shedding is enhanced by the regularly forced fluctuations that get amplified in the shear layer by the instability mechanism. The low level of turbulence in the freestream allows these fluctuations to prevail over the broadband low-energy spectrum (see Bernardini et al., 2012). These coherent structures are more effective in transporting high-momentum fluid towards the wall thus favoring reattachment.

Acoustic Control with High-*Tu*

The low-*Tu* level was chosen in order to investigate the effect on the flow of a predominant frequency dominating in a low energy broadband spectrum. On the other hand, the high-*Tu* case is more representative of a real engine environment and could indicate whether a single frequency excitation could still be "selected" by the flow even if it is buried in a high energy broadband spectrum. The two blade profiles present different levels of reverse flow without control as observed by the ensemble-averaged PIV data shown in Figure 5 (left column). The effect of turbulence level is relevant in the front-loaded profile, where the open separation resulting in the low-*Tu* case is reduced to a closed separation bubble (Figure 5 top left). As for the aft-loaded profile instead, the higher turbulent fluctuations are not able to reattach the flow resulting in a large open separation (Figure 5 bottom left). Hot-film measurements in the uncontrolled shear layer document a peak of most amplified frequency around f = 130 Hz for the aft-loaded profile. Both blades are controlled at their relative fundamental frequencies with the maximum amplitude allowed by the speaker and the resulting flow field is shown in Figure 5 right. The effect of control on the size of separation on Blade-F is almost imperceptible (Figure 5 top right), although a gain of about 13% in the wake loss coefficient can still be reached. The uncontrolled separation however is already small and the room for improvement is slight. By comparison, the separated shear layer in the aft-loaded profile is far enough from the wall to still allow a reduction in the bubble size. In Blade-A (Figure 5 bottom right) control at the fundamental frequency keeps the average shear layer closer to the wall although it is still not able to fully reattach the flow. This behavior suggests that the linear stability mechanism is still exploited even with high-*Tu* levels. However its global effect on separation is highly dependent on the distance of the shear layer from the wall.

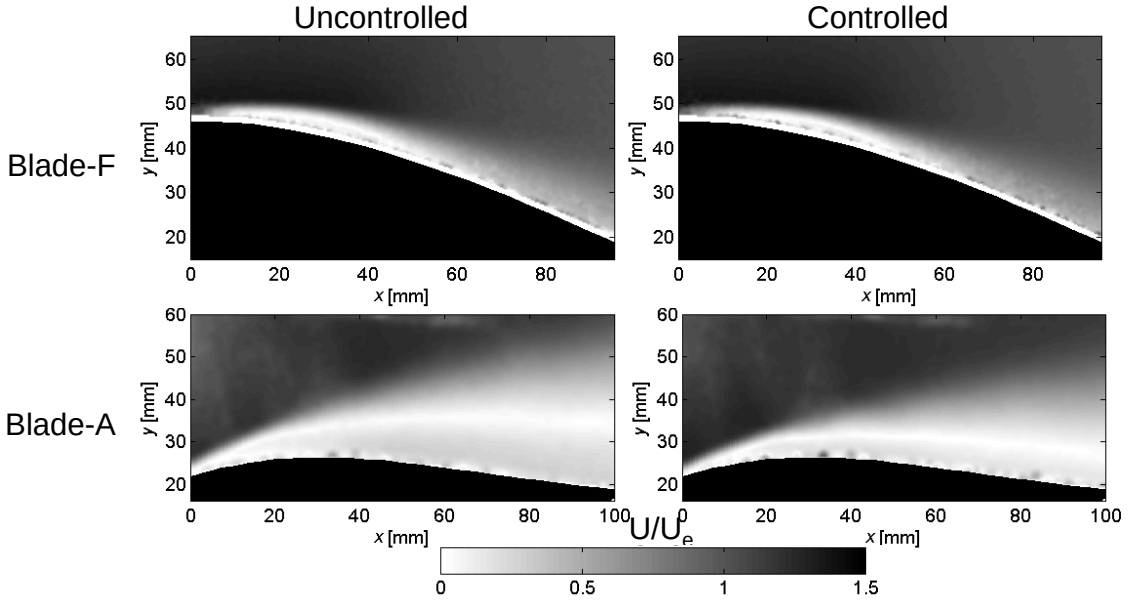

Figure 5. PIV time-averaged velocity magnitude for Blade-F (top) and Blade-A (bottom), uncontrolled (left) and controlled (right) at *f* = 110 Hz (Blade-F) and *f* = 130 Hz (Blade-A).

The effect of frequency has been assessed by wake loss coefficient and results are shown in Figure 6-left for an excitation amplitude $\Delta u_f/U_{in} \approx 0.5\%$, the same value used for the low-*Tu* case of Figure 3-left. The most effective frequencies are in the range of the fundamental frequency of the shear layer for both cases, and they span from 90 Hz to 200 Hz for Blade-F and from 110 Hz to 200 Hz for Blade-A. In this range for each blade the relative performance improvement (i.e. the normalized wake loss) considering the normalized value uncertainty of ±2.1% is about constant. This corroborates that in these excitation frequency ranges the same mechanism is triggered and the relatively small excitation amplitude used confirms that these frequencies are more effective because of the amplification of the small disturbances by linear instability mechanisms. Instability

phenomena are actually characterized not by just a pure single frequency but rather by an interval of frequencies centered on a certain value. However from the amplitude study shown in Figure 6-right it may be inferred that other frequencies can be effective although not exploiting the same linear mechanism. For both blades, acoustic excitation at the exact peak frequency - 110 Hz for Blade-F and 130 Hz for Blade-A, supposedly the most amplified frequency by linear instability - improves performances even with low amplitudes and tends to flatten out at higher amplitudes. Figure 6-right also shows the amplitude sweep for Blade-A with an excitation frequency of 90 Hz, which is investigated since it appears to have some control authority from Figure 6-left although out of the most effective frequency range. The amplitude effect at this frequency is not as significant as for 130 Hz excitation with low excitation levels, suggesting that this frequency does not get amplified in the shear layer as much as the 130 Hz frequency. On the other hand, the 90 Hz excitation appears to be more effective in separation reduction at higher amplitudes and does not reach a threshold at least for the tested values.

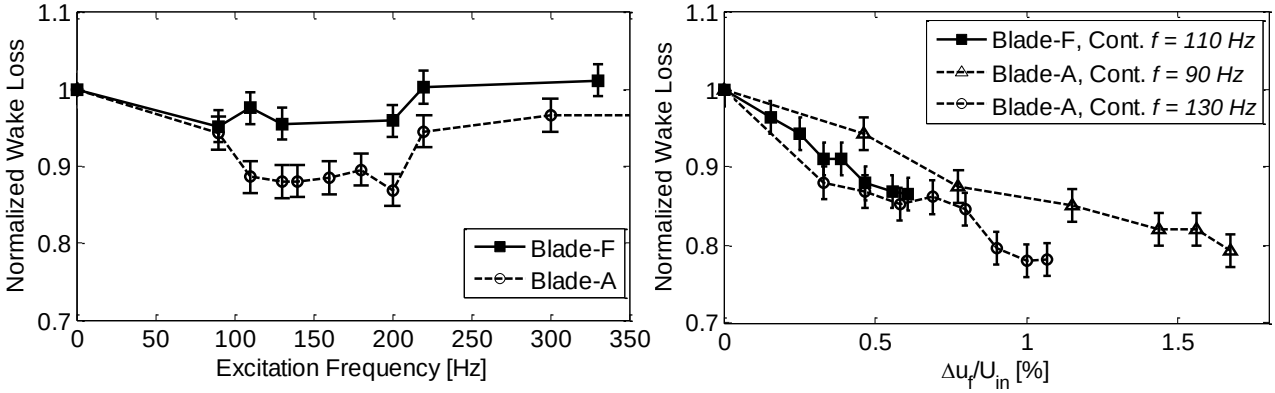

Figure 6. Integrated wake loss coefficient normalized by the uncontrolled case for Blade-F and Blade-A, High-*Tu*. Left: excitation frequency effect. Right: amplitude effect.

For Blade-A and high-*Tu* the velocity signal is collected in the shear layer at 70% C_x at a wall-normal location corresponding to the negative peak skewness of each case, in order to help understanding the mechanism of control. The PSD of the uncontrolled case (Figure 7-left) shows a peak at around 130 Hz with energy bleeding in the surrounding spectrum. When the sound is turned on at 130 Hz, the energy concentrates at this value subtracting it from the surrounding spectrum. Control at $f = 90$ Hz has the same effect of drawing energy at the excited frequency, and the natural most amplified peak ($f = 130$ Hz) disappears.

The corresponding raw signals of velocity fluctuations are plotted in Figure 7-right for 0.5 s and their wavelet analysis is shown in Figure 8. Unlike the low-*Tu* case, where intermittent wave packets at the most unstable frequencies are disrupted by almost zero-fluctuation signal (McAuliffe and Yaras, 2008), with high-*Tu* the velocity signal is rich with disturbances at all times as expected. The wavelet analysis shows however that within these highly energetic random fluctuations some wave-packets still appear at the most unstable frequency. The high amplitude fluctuations found in the raw signal in the interval $0.15 \leq t \leq 0.22$ and around $0.42 \leq t \leq 0.46$ have a frequency of about 130 Hz as shown in the wavelet plot (Figure 8-bottom). These discrete wave packets are reminiscent of K-H instability as suggested by McAuliffe and Yaras, 2010 and will eventually roll up into discrete vortices in the reattachment region. However a clear peak frequency is present only for a small amount of time, meaning that this vortex rollup at the most unstable frequency is disrupted by random fluctuations. What is really crucial for separation reduction then is not just the high level of fluctuations but the coherence of the structures, which is more effective to transport high momentum fluid toward the wall.

This is precisely where the sound excitation plays its role even with high turbulence. It collects the energy at discrete frequencies thus enhancing the coherence of vortex shedding. The velocity

fluctuations in Figure 7-right show that the signal is more regular with control at 130 Hz whereas it presents low frequency fluctuations with control at 90 Hz. The wavelet analysis in Figure 8 shows that both signals are quite regular in time, as the frequency content is concentrated around the excited frequency (marked by the bold black line) at all times. These regular frequency fluctuations feed the vortices so much so that they are continuously shed from the shear layer at constant frequency.

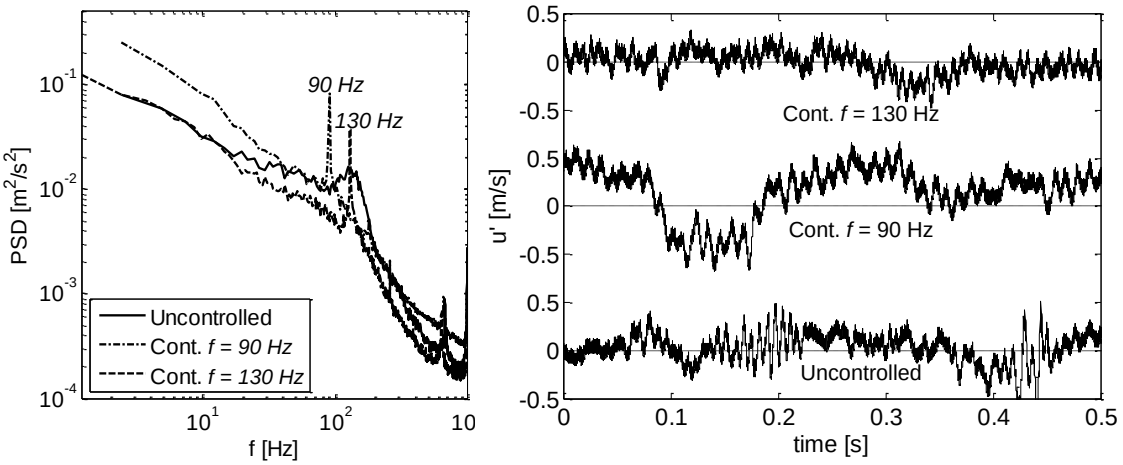

Figure 7. Left: PSD of velocity signal at 70% C_x at negative peak skewness, Right: raw velocity fluctuations signal. Blade-A, high-*Tu*, uncontrolled case and controlled cases at *f* = 90 Hz and *f* = 130 Hz.

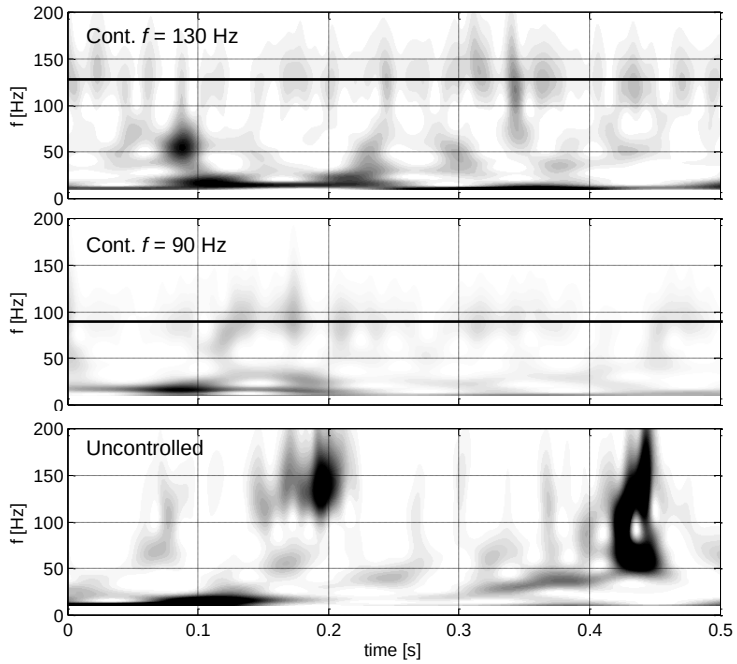

Figure 8. Wavelet power contour of velocity signal at 70% C_x at negative peak skewness. Blade-A, high-*Tu*, uncontrolled case and controlled cases at *f* = 90 Hz and *f* = 130 Hz.

The generation of coherent structures in the shear layer is assessed by phase-locked PIV data shown in Figure 9. Contours of swirl strength parameter are presented for Blade-A with high-*Tu* in the controlled cases with *f* = 90 Hz (left column) and *f* = 130 Hz (right column). Data shown in the top row are collected with excitation amplitude $\Delta u_f/U_{in} \approx 0.5\%$ while the bottom row represents data at the highest excitation amplitude tested ($\Delta u_f/U_{in} = 1.8\%$ for 90 Hz and $\Delta u_f/U_{in} = 1.1\%$ for 130 Hz). Vortex cores show up in all cases, which confirm that the excitation frequency feeds the shear

layer resulting in coherent structures shed at that frequency. It is significant that structures survive averaging over 1000 images, meaning that they lock into the forcing. At low excitation amplitude the pattern of these structures is recognizable, although the spreading and lower level of swirl contour is a sign of low coherence. The effect of increasing amplitude is that of increasing the magnitude and coherence of these vortices thus enhancing the momentum exchange between the freestream and the near-wall region. The average shear layer is therefore kept closer to the wall.

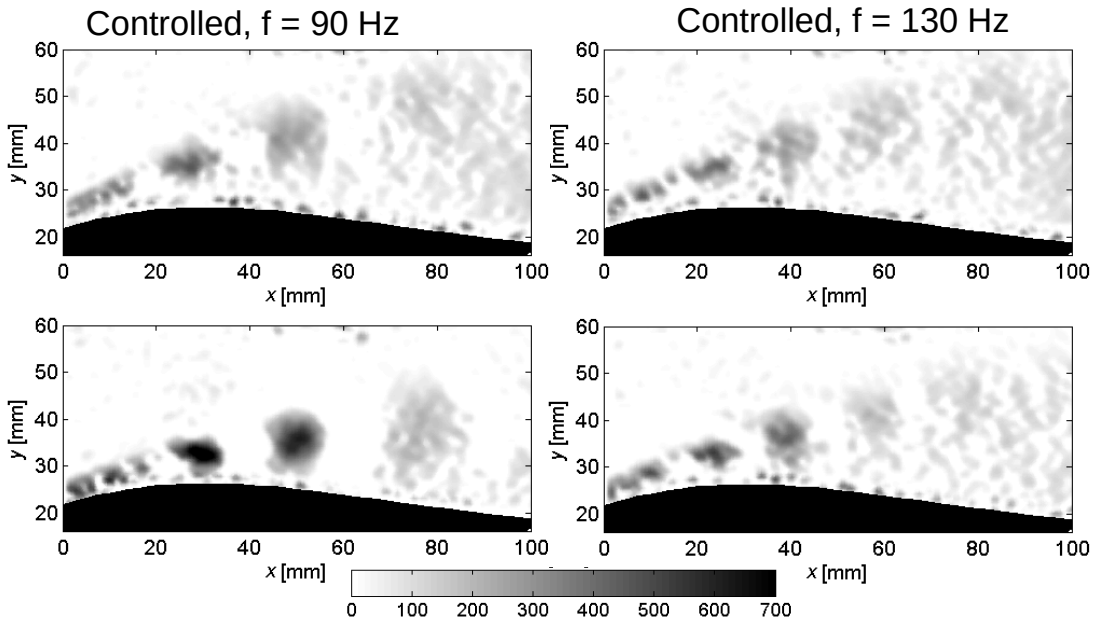

Figure 9. Contours of swirl strength parameter from phase-locked PIV, Blade-A, high-*Tu*, Control at: f = 90 Hz, $\Delta u_f/U_{in}$ = 0.5% (top left), f = 90 Hz, $\Delta u_f/U_{in}$ = 1.8% (bottom left), f = 130 Hz, $\Delta u_f/U_{in}$ = 0.5% (top right), f = 130 Hz, $\Delta u_f/U_{in}$ = 1.1% (bottom right).

CONCLUSIONS

Control of laminar separation on the suction side of two highly loaded LPT blade profiles has been accomplished by means of acoustic excitation at discrete frequencies. Hot-film measurements identified the fundamental instability frequencies in the uncontrolled shear layer. Wake pressure loss surveys demonstrated that excitation at these frequencies attains the highest performance in terms of separation reduction. The introduction of this frequency in the shear layer intensifies the coherence of shed vortical structures, thus increasing momentum exchange between the freestream and the near wall region. The effect of sound excitation is optimal with low inlet turbulence level. With high turbulence the effect of excitation on separation reduction is smaller and related to the distance from the wall of the uncontrolled shear layer. For the front-loaded profile the separation is small and acoustic forcing does not further reduce the already small separation, although some effect are still detected on the wake loss coefficient with increasing amplitudes. However, the larger separation occurring in the aft-loaded profile allows for the sound to have some effect up to about 20% wake loss reduction with the highest tested excitation amplitudes. The shear layer distance from the wall is reduced also in this case by enhanced coherence of vortical structures which are more effective to momentum exchange than the already high turbulent fluctuations. For both turbulence levels the amplitude of excitation reaches a threshold value beyond which no further improvement is achieved. At frequencies lower than the most unstable one this threshold does not seem to be reached at least for the tested amplitudes, suggesting that a different mechanism may take place. A possible explanation is the exploitation of non-linear mechanisms in the separating shear layer which will be the object of further investigations.

ACKNOWLEDGEMENTS

This work was supported by the European Union under a Marie Curie International Outgoing Fellowship for Career Development. The first author would like to acknowledge Dr. Jen-Ping Chen, The Ohio State University, Prof. Francesco Martelli, University of Florence and Prof. Marcello Manna, University of Naples Federico II for their support.

REFERENCES

Hodson, H. P., Howell, R. J., (2005), *The Role of Transition in High-Lift Low-Pressure Turbines for Aeroengines*, Prog. Aerosp. Sci., **41**(6), 419–454.

Howell, R. J., Ramesh, O. N., Hodson, H. P., Harvey, N. W., Schulte, V., (2001), *High Lift and Aft-Loaded Profiles for Low-Pressure Turbines*, J. TURBOMACH., 123, 181-188.

Corriveau, D., Sjolander, S. A., (2004), Influence of Loading Distribution on the Performance of Transonic High Pressure Turbine Blades, J. TURBOMACH., 126, 288-296.

Bons, J. P., Pluim, J., Gompertz, K., Bloxham, M., Clark, J. P., (2012), *The Application of Flow Control to an Aft-Loaded Low Pressure Turbine Cascade with Unsteady Wakes*, J. TURBOMACH., 134(3).

Bons, J. P., Sondergaard, R., Rivir, R. B., (2002), *The Fluid Dynamics of LPT Blade Separation Control Using Pulsed Jets*, J. TURBOMACH., 124(1), 77–85.

Postl, D., Balzer, W., Fasel, H. F., (2011), Control of Laminar Separation Using Pulsed Vortex Generator Jets: Direct Numerical Simulations, J. Fluid Mech., 676, 81-109.

Michalke, A., (1965), On Spatially Growing Disturbances in an Inviscid Shear Layer, J. Fluid Mech, 23, 521-544.

Watmuff, J. H., (1999), Evolution of a wave packet into vortex loops in a laminar separation bubble, J. Fluid Mech., 397, 119–169.

Baumann, J., Rose, M., Ries, T., Staudacher, S., Rist, U., (2011), *Actuated Transition in an LP Turbine Laminar Separation: an Experimental Approach*, ASME Paper GT2011-45852.

Zaman, K. B. M. Q., (1992), Effect of Acoustic Excitation on Stalled Flows over an Airfoil, AIAA J., 30(6), 1492-1499.

Greenblatt, D., Wygnanski , I. J., (2000), *The control of flow Separation by Periodic Excitation*, Prog. Aerosp. Sci., 36(7), 487-545

Yarusevych, S., Sullivan, P. E., Kawall, J. G., (2007), Effect of Acoustic Excitation Amplitude on Airfoil Boundary Layer and Wake Development, AIAA J., 45(4), 760-771.

Benton, S. I., Bons, J. P, Sondergaard, R., (2013), Secondary Flow Loss Reduction Through Blowing for a High-Lift Front-Loaded Low Pressure Turbine Cascade, J. TURBOMACH. 135, 021020.

Farge, M., (1992) *Wavelet Transforms and their Applications to Turbulence*, Annu. Rev. Fluid Mech., 24, 395-457.

Torrence, C., Compo, G.P., (1998), *A Practical Guide to Wavelet Analysis*, B. Am. Meteorol. Soc., 79(1), 61-78.

Adrian,R.J.,Christensen,K. T.,Liu,Z.–C., (2000) *Analysis and Interpretation of Instantaneous Turbulent Velocity Fields*, Exp. Fluids, Vol. 29(3), 275-290.

Zhou, J, Adrian, R. J., Balachandar, S., Kendall, T. M., (1999), *Mechanisms for generating coherent packets of hairpin vortices in channel flow,* J. Fluid Mech., 387, 353-396.

Bernardini, C., Benton, S. I., Bons, J. P. (2012), The Effect of Acoustic Excitation on Boundary Layer Separation of a Highly Loaded LPT Blade, ASME Paper GT2012-69618.

McAuliffe, B.R., Yaras, M. I., (2010), Transition Mechanisms in Separation Bubbles under Low- and Elevated-Freestream Turbulence, J. TURBOMACH., 132(1)

McAuliffe, B. R., Yaras, M. I., (2008), Numerical Study of the Instability Mechanisms Leading to Transition in Separation Bubbles, J. TURBOMACH., 130(2).